SUPPLEMENTAL FIGURES

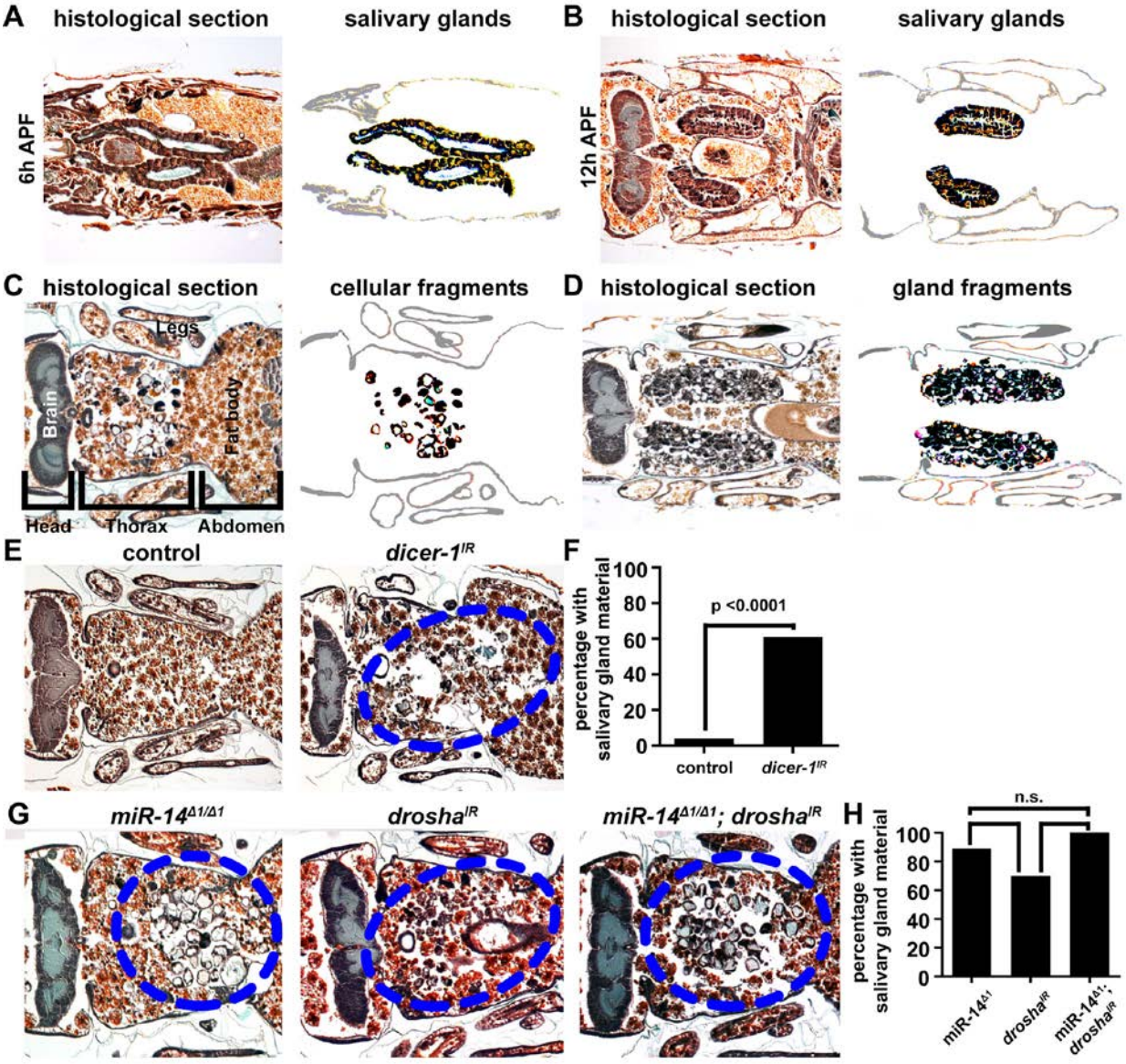

Figure S1. A description of salivary gland degradation during development, cellular and gland fragments, *dicer-1* is required for salivary gland degradation, and *drosha* functions in the same pathway as *miR-14*. Related to Figure 1

(A) A histological section (left) of a wild type animal 6 h after puparium formation approximately 8-10 hours before complete gland degradation. The left side of all images is the

anterior end of the animal. The image on the right shows emphasized salivary glands with all other material removed.

(B) A histological section (left) of a wild type animal 12 h after puparium formation approximately 2-4 hours before complete gland degradation. The image on the right shows emphasized salivary glands with all other material removed.

(C) A histological section (left) 24 h after puparium formation of an animal that partially, but not completely, degraded its salivary glands thereby displaying a cellular fragment phenotype (*fkh*-GAL4/*w*; +/UAS-*drosha*^{IR}). Labeled are the head (left part of the animal), thorax (middle part of the animal), abdomen (right part of the animal), the brain (blue stained tissue), fat body cells (brown and red stained cells), and developing legs. The image on the right shows the cellular fragments with all other material removed. Note these cellular fragments have remained 10 h after they should have been degraded.

(D) A histological section (left) 24 h after puparium formation of an animal failed to degrade its salivary glands thereby displaying a salivary gland fragment phenotype (*w*; *miR-14*$^{\Delta 1}$/*miR-14*$^{\Delta 1}$; UAS-p35/*fkh*-GAL4). The image on the right shows the gland fragments with all other material removed. Note these gland fragments have remained 10 h after they should have been degraded.

(E) Samples from control animals (*+/w; +/*UAS-*dicer-1*^{IR}), *n* = 27 (left), and those with salivary gland-specific knockdown of *dicer-1* (*fkh*-GAL4/*w*; +/UAS-*dicer-1*^{IR}), *n* = 28 (right), analyzed by histology for the presence of salivary gland material (blue dotted circle) 24 h after puparium formation.

F) Quantification of data from (E). Data are represented as mean. Statistical significance was determined using a Chi-squared test.

(G) Samples from *miR-14* mutant animals (*w*; *miR-14*$^{\Delta 1}$/*miR-14*$^{\Delta 1}$;+/UAS-*drosha*^{IR}), *n* = (left), animals with salivary gland-specific knockdown of *drosha* (*w*; +/*miR-14*$^{\Delta 1}$; *fkh*-GAL4/UAS-*drosha*^{IR}), *n* = 23 (middle), and *miR-14* mutant animals with salivary gland-specific knockdown of *drosha* (*w*; *miR-14*$^{\Delta 1}$/*miR-14*$^{\Delta 1}$; *fkh*-GAL4/UAS-*drosha*^{IR}), *n*= 20, analyzed by histology for the presence of salivary gland material (blue dotted circle) 24 h after puparium formation.
(H) Quantification of data from (G). Data are represented as mean. Statistical significance was determined using a Chi-squared test.

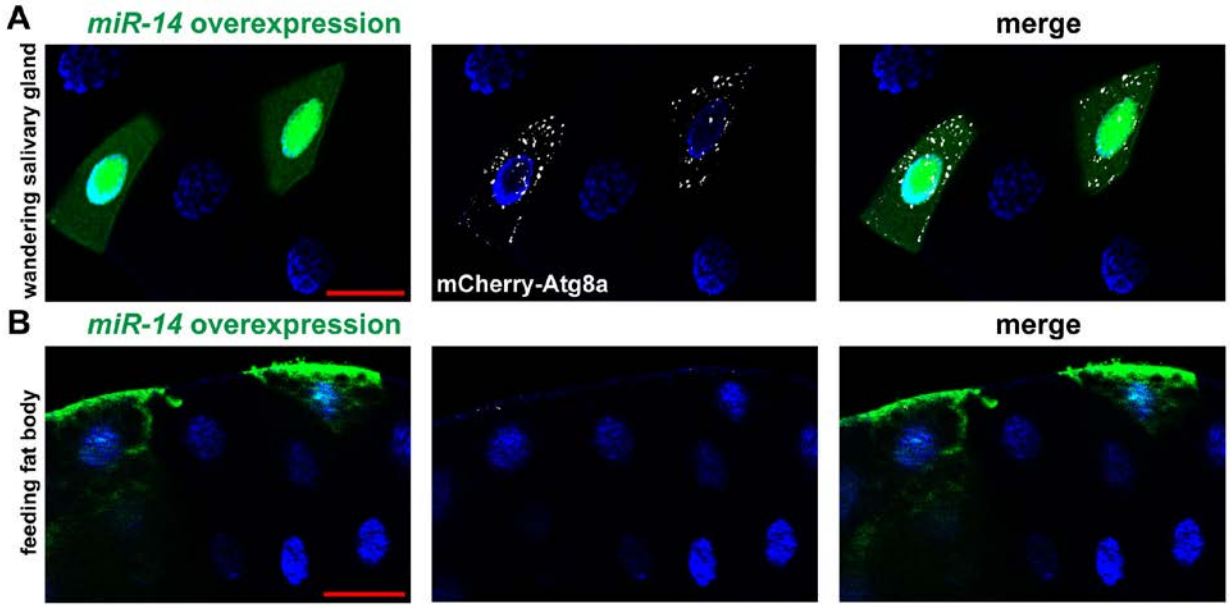

Figure S2. Mis-expression of *miR-14* is sufficient to induce autophagy in the salivary gland, but not in the fat body. Related to Figure 3

(A and B) Salivary glands dissected from wandering larvae (A) and fat bodies dissected from feeding larvae (B) expressing mCherry-Atg8a in all cells, and *miR-14* mis-expression specifically in GFP-marked clone cells (hsflp/*w*; pmCherry-Atg8a/+; *act*<FRT, cd2, FRT>Gal4, UAS-GFP/UAS-*luciferase-miR-14*) analyzed for mCherry-Atga8a puncta. Salivary glands and fat bodies were all stained with Hoechst (blue). Scale bars represent 50µm.

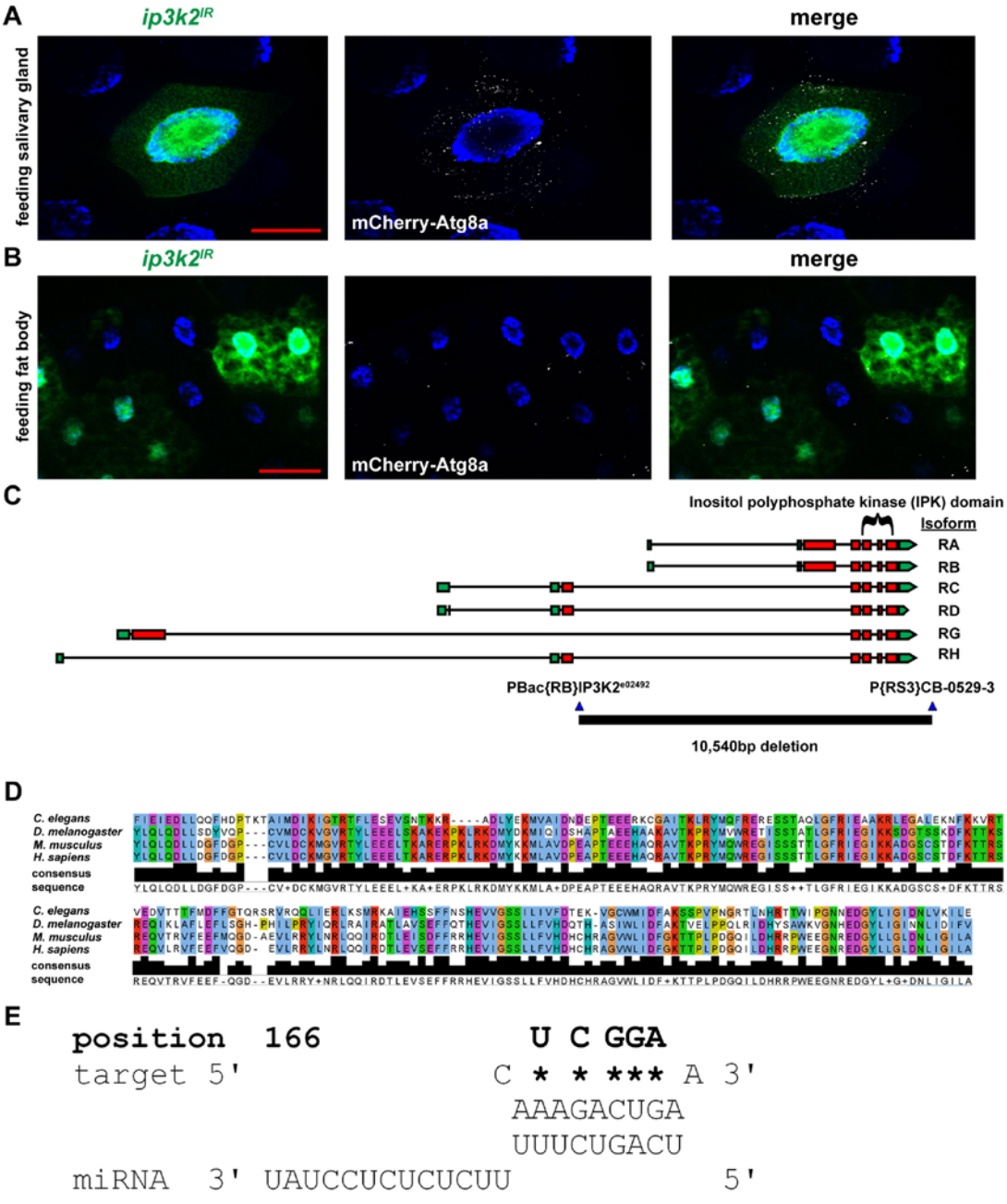

Figure S3. *ip3k2* RNAi is sufficient to induce autophagy in the salivary gland, *ip3k2* deletion mutant, the conserved IPK domain of IP3K2, and the predicted *miR-14* binding site in *ip3k2*. Related to Figure 4

(A and B) Salivary glands (A) and fat bodies (B) expressing mCherry-Atg8a in all cells, and *ip3k2*^{IR} knockdown specifically in GFP-marked clone cells (hsflp/*w*; pmCherry-Atg8a/+;

act<FRT, cd2, FRT>Gal4, UAS-GFP/UAS-*ip3k2*^{IR}) dissected from feeding larvae for analyses of mCherry-Atg8a puncta. Salivary glands and fat bodies were all stained with Hoechst (blue). Scale bars represent 50µm.

(C) The two flippase recognition target (FRT) containing elements, PBac{RB}IP3K2^{e02492} and P{RS3}CB-0529-3 were recombined together to create the *ip3k2*$^{\Delta 1}$ allele containing a 10,540bp genomic deletion that deletes isoforms A and B, and most of isoforms C through H including the IPK domain of all isoforms.

(D) Alignment of the highly conserved IPK domain. The *C. elegans* protein is lfe-1. The *D. melanogaster* protein is IP3K2. The *M. musculus* and *H. sapiens* proteins are both ITPKA.

(E) The *miR-14* binding site in the 3' UTR of *ip3k2*. The nucleotides replaced in the mutated sensor line are indicated with *, and the new nucleotides are shown above.

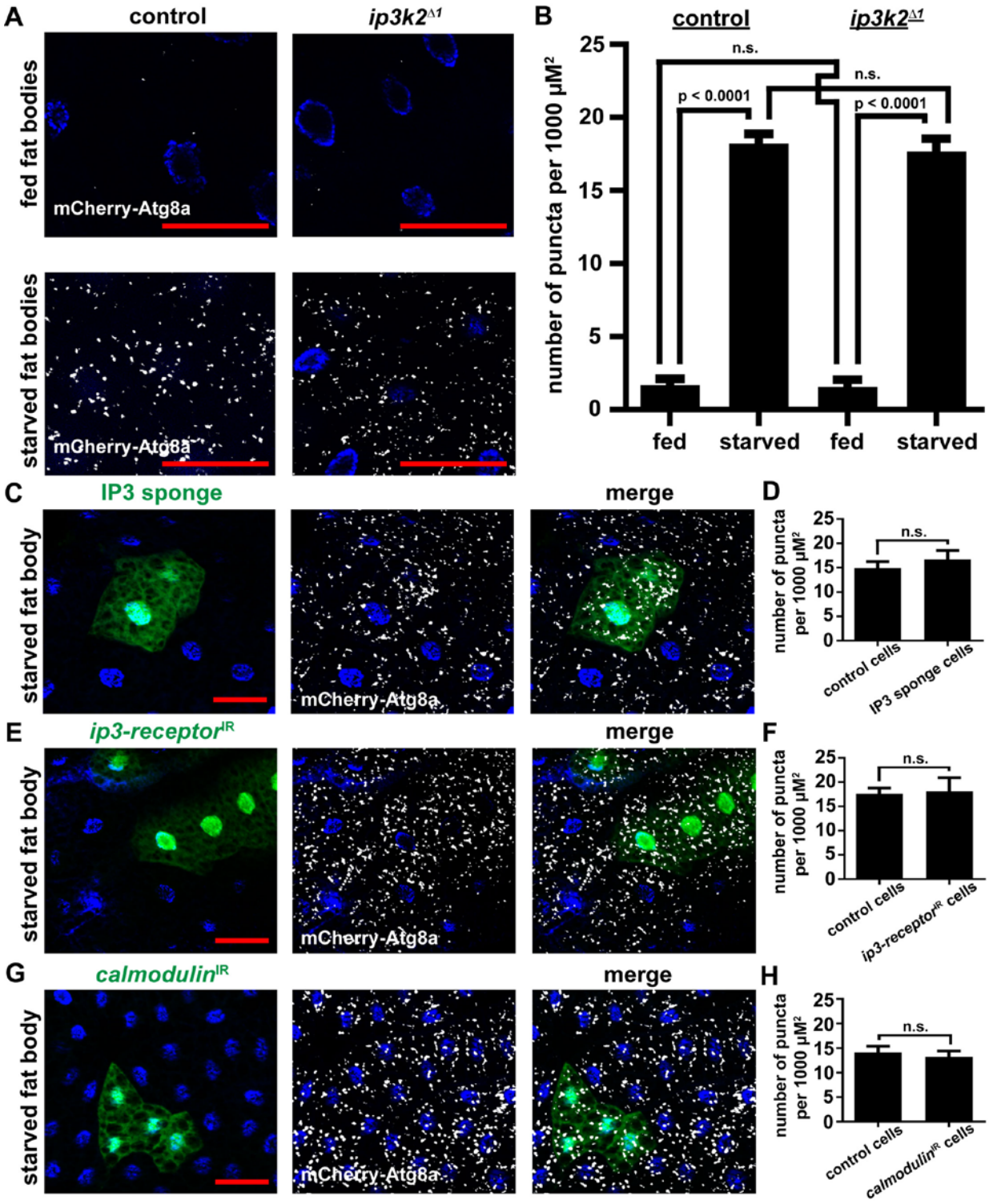

Figure S4. The *ip3k2* mutant, IP3 sponge, *ip3-receptor* and *Calmodulin* knockdowns are not sufficient to alter stress induced autophagy in the fat body. Related to Figure 4

(A) mCherry-Atg8a was expressed in the fat bodies of control animals (left) (*w*/*ip3k2*$^{\Delta 1}$; +/pmCherry-Atg8a) and in *ip3k2*$^{\Delta 1}$ mutant animals (right) (*ip3k2*$^{\Delta 1}$/Y; +/pmCherry-Atg8a). Animals were either fed (top) or starved for 4 h (bottom), and fat bodies were dissected for analyses of mCherry-Atg8a puncta.

(B) Quantification of data from (A). Data are represented as mean +/- SEM; $n \geq 10$. Statistical significance was determined using a Student's t-test.

(C) Fat bodies expressing mCherry-Atg8a in all cells, and the IP3 sponge specifically in GFP-marked clone cells (hsflp/*w*; pmCherry-Atg8a/+; *act*<FRT, cd2, FRT>Gal4, UAS-GFP/UAS-IP3 sponge) dissected from 4 h starved larvae for analyses of mCherry-Atg8a puncta.

(D) Quantification of data from (C). Data are represented as mean +/- SEM; $n = 8$. Statistical significance was determined using a Student's t-test.

(E) Fat bodies expressing mCherry-Atg8a in all cells, and knockdown of the *ip3-receptor* specifically in GFP-marked clone cells (hsflp/*w*; pmCherry-Atg8a/UAS-*ip3-receptor*^{IR}; *act*<FRT, cd2, FRT>Gal4, UAS-GFP/+) dissected from 4 h starved larvae for analyses of mCherry-Atg8a puncta.

(F) Quantification of data from (E). Data are represented as mean +/- SEM; $n = 7$. Statistical significance was determined using a Student's t-test.

(G) Fat bodies expressing mCherry-Atg8a in all cells, and knockdown of *Calmodulin* specifically in GFP-marked clone cells (hsflp/*w*; pmCherry-Atg8a/+; *act*<FRT, cd2, FRT>Gal4, UAS-GFP/UAS-*Calmodulin*^{IR}) dissected from 4 h starved larvae for analyses of mCherry-Atg8a puncta.

(H) Quantification of data from (G). Data are represented as mean +/- SEM; $n = 8$. Statistical significance was determined using a Student's t-test.

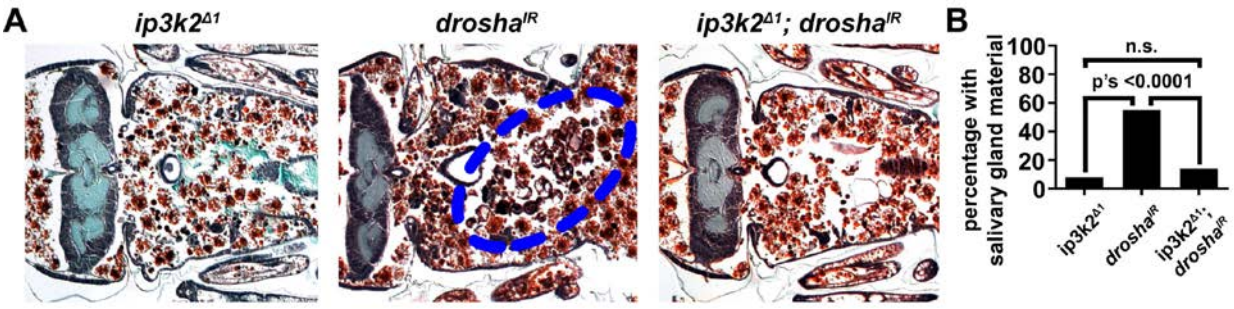

Figure S5. *ip3k2* functions genetically downstream of *drosha.* Related to Figure 4

(A) Samples from *ip3k2* mutant animals (*ip3k2*$^{\Delta 1}$/Y; +/UAS-*drosha*^{IR}), *n* = 24 (left), animals with salivary gland-specific knockdown of *drosha* (*ip3k2*$^{\Delta 1}$/+; *fkh*-GAL4/UAS-*drosha*^{IR}), *n* = 20 (middle), and *ip3k2* mutant animals with salivary gland-specific knockdown of *drosha* (*ip3k2*$^{\Delta 1}$/Y; *fkh*-GAL4/UAS-*drosha*^{IR}), *n* = 21, analyzed by histology for the presence of salivary gland material (blue dotted circle) 24 h after puparium formation.

(B) Quantification of data from (A). Data are represented as mean. Statistical significance was determined using a Chi-squared test.

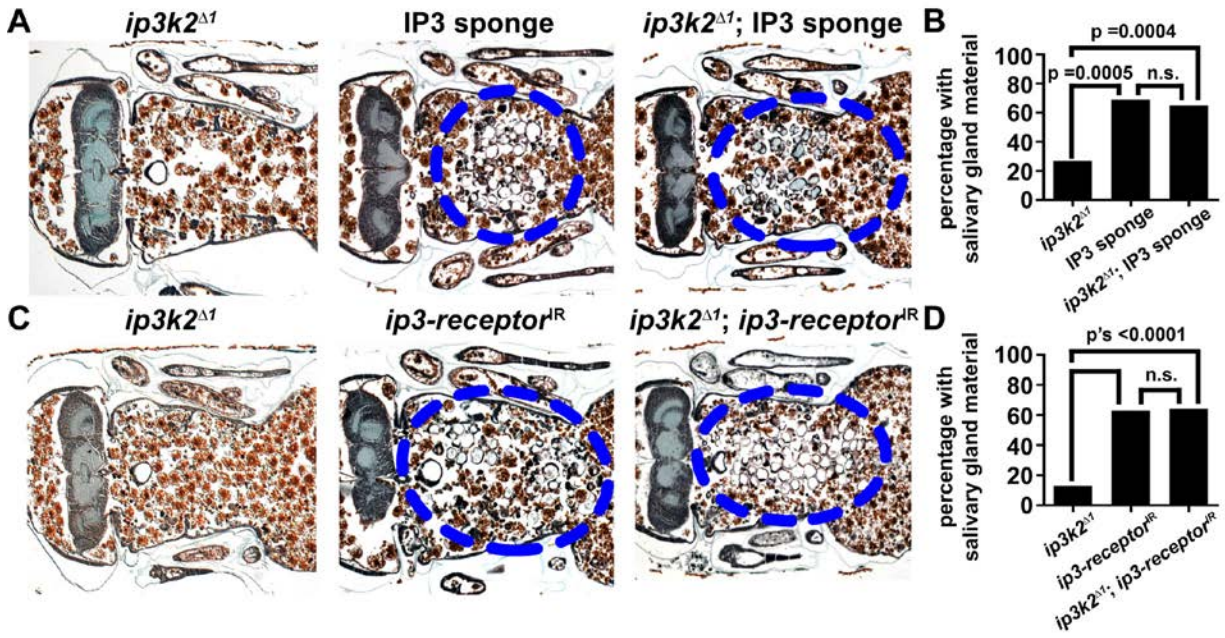

Figure S6. IP3 signaling is required for salivary gland degradation and function downstream of *ip3k2*. Related to Figure 5

(A) Samples from *ip3k2* mutant animals (*ip3k2*$^{\Delta 1}$/Y; +/UAS-IP3 sponge), *n* = 22 (left), animals with salivary gland-specific expression of the IP3 sponge (*ip3k2*$^{\Delta 1}$/*w*; *fkh*-GAL4/UAS-IP3 sponge), *n* = 16 (middle), and *ip3k2* mutant animals with salivary gland-specific expression of the IP3 sponge (*ip3k2*$^{\Delta 1}$/Y; *fkh*-GAL4/UAS-IP3 sponge), *n* = 20 (right), analyzed by histology for the presence of salivary gland material (blue dotted circles) 24 h after puparium formation.

(B) Quantification of data from (A). Data are represented as mean. Statistical significance was determined using a Chi-squared test.

(C) Samples from *ip3k2* mutant animals (*ip3k2*$^{\Delta 1}$/Y; +/UAS-*ip3-receptor*^{IR}), *n* = 16 (left), animals with salivary gland-specific knockdown of the *ip3-receptor* (*ip3k2*$^{\Delta 1}$/*w*; +/UAS-*ip3-receptor*^{IR}*; fkh*-GAL4/+), *n* = 27 (middle), and *ip3k2* mutant animals with salivary gland-specific knockdown of the *ip3-receptor* (*ip3k2*$^{\Delta 1}$/Y; +/UAS-*ip3-receptor*^{IR}*; fkh*-GAL4/+), *n* = 22 (right),

analyzed by histology for the presence of salivary gland material (blue dotted circles) 24 h after puparium formation.

(D) Quantification of data from (C). Data are represented as mean. Statistical significance was determined using a Chi-squared test.

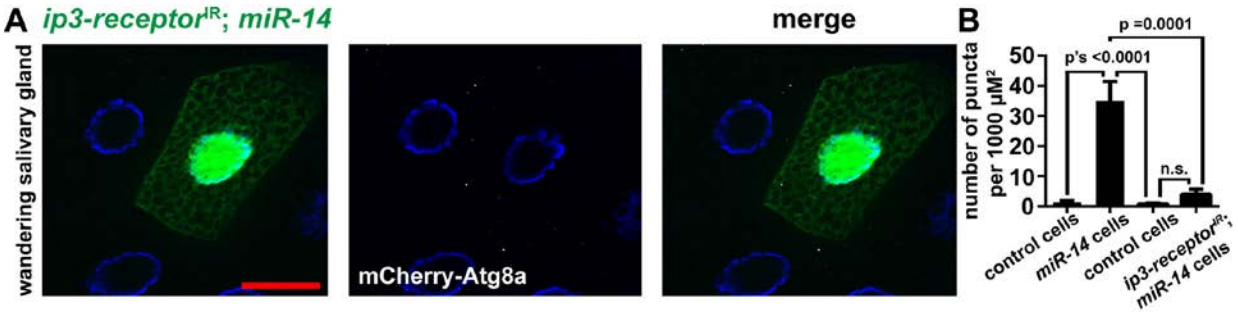

Figure S7. Knockdown of the *ip3-receptor* in the salivary gland is sufficient to suppress the induction of autophagy by *miR-14* mis-expression. Related to Figures 3 and 5

(A) A salivary gland expressing mCherry-Atg8a in all cells, and knockdown of the *ip3-receptor* as well as mis-expression of *miR-14* specifically in GFP-marked clone cells (hsflp/*w*; pmCherry-Atg8a/UAS-*ip3-receptor*^{IR}; *act*<FRT, cd2, FRT>Gal4, UAS-GFP/UAS-*luc-miR-14*) dissected from wandering larvae for analyses of mCherry-Atg8a puncta.

(B) Quantification of data from Figure S2A (first two columns) and (A) (last two columns). Data are represented as mean +/- SEM; $n \geq 9$. Statistical significance was determined using a Student's t-test.

Table S1. microRNA levels in the salivary gland during cell death. Related to Figure 1

	Hours after puparium formation				
microRNA	6	8	10	12	14
dme-miR-1	11.16457833	8.96409467	10.38516	9.78672	10.77394
dme-miR-2a	12.281498	9.62075467	10.72464	10.39966	10.7852
dme-miR-2b	10.79751833	8.04892467	11.06917	8.64838	9.76797
dme-miR-2c	undetected	undetected	undetected	undetected	undetected
dme-miR-3	undetected	undetected	undetected	undetected	undetected
dme-miR-4	undetected	undetected	undetected	undetected	undetected
dme-miR-5	undetected	undetected	undetected	undetected	undetected
dme-miR-6	undetected	undetected	undetected	undetected	undetected
dme-miR-7	undetected	11.64106467	undetected	undetected	undetected
dme-miR-8	9.537857667	6.12127467	8.64859	6.84268	9.1936
dme-miR-9a	12.27861967	8.38115467	12.22185	undetected	undetected
dme-miR-9b	13.152634	10.16113467	12.85452	undetected	undetected
dme-miR-9c	undetected	11.38323467	13.02512	11.34856	undetected
dme-miR-10	undetected	undetected	undetected	undetected	undetected
dme-miR-11	10.10956867	8.45094467	10.18735	8.30703	9.40849
dme-miR-12	9.986912667	9.00629467	9.59349	8.07788	11.06808
dme-miR-13a	undetected	undetected	undetected	undetected	undetected
dme-miR-13b	11.911716	9.18659467	10.4429	8.67231	9.99911
dme-miR-14	10.64355733	7.42450467	8.86879	7.52733	9.41584
dme-miR-31a	undetected	12.43609467	undetected	undetected	undetected
dme-miR-31b	undetected	undetected	undetected	undetected	undetected
dme-miR-33	undetected	undetected	undetected	undetected	undetected
dme-miR-34	undetected	13.00962467	12.82689	11.4035	undetected
dme-miR-79	undetected	undetected	undetected	11.38347	undetected
dme-miR-87	undetected	undetected	undetected	undetected	undetected
dme-miR-92a	undetected	11.98784467	undetected	undetected	undetected
dme-miR-92b	undetected	11.63027467	undetected	undetected	undetected
dme-miR-100	undetected	11.58414467	undetected	undetected	undetected
dme-miR-124	undetected	undetected	undetected	undetected	undetected
dme-miR-125	undetected	10.79810467	12.3666	10.27391	undetected
dme-miR-133	undetected	undetected	undetected	undetected	undetected
dme-miR-184	undetected	9.13495467	13.10597	9.55139	8.75563
*dme-miR-184**	undetected	undetected	undetected	undetected	undetected
dme-miR-210	undetected	undetected	undetected	undetected	undetected
dme-miR-219	undetected	undetected	undetected	undetected	undetected
dme-miR-263a	undetected	undetected	12.9377	undetected	undetected
dme-miR-263b	undetected	undetected	undetected	undetected	undetected
dme-miR-274	undetected	undetected	undetected	undetected	undetected
dme-miR-275	8.629958333	7.22112467	7.87684	8.04112	8.12283
dme-miR-276a	8.528196	6.18353467	8.17634	7.03379	6.34527
*dme-miR-276a**	undetected	undetected	undetected	undetected	undetected
dme-miR-276b	11.51158333	8.17866467	10.09851	9.83226	7.60686
dme-miR-277	13.19924933	10.40040467	undetected	10.03176	undetected
dme-miR-278	undetected	undetected	undetected	undetected	undetected
dme-miR-279	undetected	11.95146467	12.96985	11.31981	undetected
dme-miR-280	undetected	undetected	12.88042	undetected	undetected
dme-miR-281	undetected	undetected	undetected	undetected	undetected
*dme-miR-281-1**	undetected	undetected	undetected	undetected	undetected
dme-miR-282	undetected	undetected	undetected	undetected	undetected
dme-miR-283	undetected	undetected	undetected	undetected	undetected
dme-miR-284	undetected	undetected	undetected	undetected	undetected
dme-miR-285	undetected	undetected	undetected	undetected	undetected
dme-miR-286	undetected	undetected	undetected	undetected	undetected
dme-miR-287	undetected	undetected	undetected	undetected	undetected
dme-miR-288	undetected	undetected	undetected	undetected	undetected
dme-miR-289	11.747825	8.57399467	8.35656	8.25614	9.88747

dme-miR-303	undetected	undetected	undetected	undetected	undetected
dme-miR-304	10.48159333	9.34134467	9.65785	7.96495	undetected
dme-miR-305	undetected	9.96978467	10.83799	9.61609	undetected
dme-miR-306	undetected	undetected	undetected	undetected	undetected
*dme-miR-306**	undetected	undetected	undetected	undetected	undetected
dme-miR-307	9.221936	7.69138467	7.95909	6.89493	6.42864
dme-miR-308	undetected	undetected	undetected	undetected	undetected
dme-miR-309	undetected	undetected	undetected	undetected	undetected
dme-miR-310	undetected	undetected	undetected	undetected	undetected
dme-miR-311	undetected	undetected	undetected	undetected	undetected
dme-miR-312	undetected	undetected	undetected	undetected	undetected
dme-miR-313	undetected	undetected	undetected	undetected	undetected
dme-miR-314	undetected	undetected	undetected	undetected	undetected
dme-miR-315	undetected	undetected	undetected	undetected	undetected
dme-miR-316	undetected	undetected	undetected	undetected	undetected
dme-miR-317	undetected	undetected	undetected	undetected	undetected
dme-miR-318	undetected	undetected	undetected	undetected	undetected
dme-miR-iab-4-3p	undetected	undetected	undetected	undetected	undetected
dme-miR-iab-4-5p	undetected	undetected	undetected	undetected	undetected
dme-miR-bantam	11.69185933	10.48656467	11.156	10.83246	undetected
dme-miR-let7	13.33426933	11.49732467	undetected	undetected	undetected

---

Total RNA was extracted from dissected wild type (Canton S) salivary glands staged at 6, 8, 10, 12 and 14 h after puparium formation. TaqMan was used to profile 77 microRNAs for presence in the salivary gland. ΔCT was normalized to 2s RNA and is listed for each microRNA that was profiled at each time point.

Table S2. List of RNAi lines screened to identify targets of *miR-14*. Related to Figure 4

Gene	RNAi line
Activity-regulated cytoskeleton associated protein 1	Bloomington TRiP 25954
Aspartyl-tRNA synthetase	VDRC TID 7750
bip1	VDRC TID 26104
calcium-binding protein 1	VDRC TID 108439
Cdk12	VDRC TID 25508
center divider	VDRC TID 43634
cg11367	VDRC TID 26141
CG6793	VDRC TID 101148
CG6954	VDRC TID 27759
CG8258	VDRC TID 45790
Ecdysone-induced protein 75B	VDRC TID 108399
Ecdysone receptor	VDRC TID 37059
GalNAc-T1	VDRC TID 37174
hairy	Bloomington TRiP 34326
Hormone-receptor-like in 78	VDRC TID 109435
I'm not dead yet	VDRC TID 9981
Innexin 3	VDRC TID 39094
Inositol 1,4,5-trisphosphate kinase 1	Bloomington TRiP 31733 and Terhzaz et al.
Inositol 1,4,5-trisphosphate kinase 2	VDRC TIDs 19159 and 102772
inscuteable	Bloomington TRiP 35042
Ionotropic receptor 76a	Bloomington TRiP 34678
Lsm11	VDRC TID 20280
Mesoderm-expressed 2	Bloomington TRiP 32460
mushroom-body expressed	VDRC TID 28024
rhomboid	Bloomington TRiP 28609
roughest	Bloomington TRiP 28672
small optic lobes	Bloomington TRiP 29463
sugarbabe	Bloomington TRiP 55182
Sulfated	VDRC TID 37361
vrille	VDRC TID 5650
X11L	VDRC TID 27429

RNAi lines screened for clonal induction of pmCherry-Atg8a puncta in dissected wandering larval salivary glands, but not in feeding larval fat bodies. RNAi lines were crossed with hsflp; pmCherry-Atga8a; *act*<FRT, cd2, FRT>Gal4, UAS-GFP.

SUPPLEMENTAL EXPERIMENTAL PROCEDURES

Drosophila strains

The Canton-S strain was used as the wild-type control. *miR-14*$^{\Delta 1}$(Xu et al., 2003), *miR-9a*^{e39} *and miR-9a*^{j22} (Li et al., 2006), *miR-8*$^{\Delta 2}$ (Karres et al., 2007), *miR-7*$^{\Delta 1}$ (Li and Carthew, 2005), *let-7*$^{KO.C}$ (Caygill and Johnston, 2008), *let-7*^{K01} and *let-7*^{GKI} (Sokol et al., 2008), *miR-278*^{KO} (Teleman et al., 2006), *miR-279*$^{S0962\text{-}7}$ and *miR-279*$^{\Delta 0.8}$ (Cayirlioglu et al., 2008), *pWiz-drosha*$^{IR\#2}$ (from P. Zamore) and UAS-*dicer-1*^{IR} (Bloomington *Drosophila* stock center line 28598) were used for analyses of microRNA function. The following Vienna *Drosophila* RNAi Center (VDRC) stocks were used: UAS-*Atg6*^{IR} VDRC Transformant ID (TID) 22122, UAS-*ip3k2*^{IR} VDRC TID 102772, UAS-*ip3k2*^{IR} VDRC TID 19159. The sequences used for VDRC knock-down strains are available for each TID at http://stockcenter.vdrc.at/control/main. For mis-expression studies, we used UAS-*miR-14* (Xu et al., 2003), UAS-*luciferase-miR-14* (Bloomington *Drosophila* stock center line 41178) and UAS-p35 (Hay et al., 1994). For clonal mis-expression and RNAi studies we used hsflp; +; *act*<FRT, cd2, FRT>Gal4, UAS-GFP (Bloomington *Drosophila* stock center). All RNAi lines used to screen for targets of *miR-14* are listed in Supplementary Table 2. pmCherry-Atg8a was used as a marker of autophagy (Denton et al., 2012), and tGPH was used as a reporter of phosphatidylinositol-3, 4, 5-P3 (Britton et al., 2002). *tub*-eGFP-*ip3k2* wild type 3'UTR and *tub*-eGFP-*ip3k2* mutated 3'UTR lines were used as sensors for regulation of the *ip3k2* 3'UTR by *miR-14*. The *ip3k2* mutant allele *ip3k2*$^{\Delta 1}$ was created for this paper. UAS-IP3-sponge^{M49} (Usui-Aoki et al., 2005), UAS-*ip3-receptor*^{IR} (VDRC TID 106982), and UAS-*calmodulin*^{IR} (Bloomington *Drosophila* stock center line 34609) were used for analysis of IP3 signaling and *Calmodulin*. UAS-GCaMP5 strains were used for live-imaging of calcium (Bloomington *Drosophila* stock center lines 42037 and 42038).

ip3k2$^{\Delta 1}$ mutant

The *ip3k2*$^{\Delta 1}$ deletion allele was created by flippase mediated site specific recombination of the lines PBac{RB}IP3K2^{e02492} (Bloomington *Drosophila* stock center 18060) and P{RS3}CB-0529-3 (*Drosophila* Genetic Resource Center line number 123222), resulting in a 10,540 base pair deletion from genomic locations X:13,213,313 to 13,223,853 while leaving a 2,241 base pair hybrid PBac{RB}/P{RS3} element, and was subsequently out crossed three times to wild-type strain. The deletion was validated by two rounds of PCR amplification using the primers 5'-CCGCCGAAGATTGCGTTGATTACACT-3' and 5'-GTCCCCTTGAAATCTCGCTGTGACTG-3'for the first round and the primers 5'-GTATCCATCCTCGTCGC-3' and 5'-CTTTCGCACAAACAAACCTT-3' for the second round, and the final product was TOPO cloned. The TOP clone was then sequenced using the primers 5'-CTTTCTAGAGAATAGGAACTTC-3', 5'-GAAGTTCCTATTCTCTAGAAAG-3', and the TOPO cloning primers m13 forward and m13 reverse to validate the deletion.

Transgenic strains

To generate the *tub*-eGFP-*ip3k2* wild type 3'UTR vector, the 3'UTR of *ip3k2* was amplified from genomic DNA using the primers 5'-GATATTCTAGAATCCATACATTTCCACACGGAGG-3' and 5'-GATATCTCGAGCACTGGTCGTCATTTTGCCG-3' and ligated into the XbaI-XhoI the cut *tub*-eGFP vector (from E. Lai). The attB sequence was amplified from the pUAST-attB vector (GenBank: EF362407 1) by using the primers 5'-GATATCTCGAGGATCCACTAGTGTCGACGATGT-3' and 5'-

GATATCTCGAGTGGCTAGAACTAGTGTCGACAT-3' and ligated into the EcoRI cut *tub*-eGFP-*ip3k2* 3'UTR vector. The *miR-14* binding site was mutated via *de novo* gene synthesis (Biomatik). The sequence

TCTAGAATCCATACATTTCCACACGGAGGTTTGGGGCTGGGCCCCGGAGA

CAAAGACATTTCCAATTTCCGAATCGATTAATCCCCAATTCCTAGGCTTA

GTTATACATTTTTTTTTTGTTTTTTTCTAACAGTTTGCGTACATTTAACC

CCTTAAGTTTAAAATCATACAGGAAAATCACAATATGCATACACATATTTTTTAATA

TATACGATATACGCGT was ligated into the XbaI and MluI cut wild type sensor vector. Construct sequences were validated and inserted into the attP2 landing site to generate transgenic *Drosophila* lines (Genetic Services, Inc).

SUPPLEMENTAL REFERENCES

Britton, J.S., Lockwood, W.K., Li, L., Cohen, S.M., and Edgar, B.A. (2002). Drosophila's insulin/PI3-kinase pathway coordinates cellular metabolism with nutritional conditions. Dev Cell *2*, 239-249.

Caygill, E.E., and Johnston, L.A. (2008). Temporal regulation of metamorphic processes in Drosophila by the let-7 and miR-125 heterochronic microRNAs. Curr Biol *18*, 943-950.

Cayirlioglu, P., Kadow, I.G., Zhan, X., Okamura, K., Suh, G.S., Gunning, D., Lai, E.C., and Zipursky, S.L. (2008). Hybrid neurons in a microRNA mutant are putative evolutionary intermediates in insect CO2 sensory systems. Science *319*, 1256-1260.

Denton, D., Chang, T.K., Nicolson, S., Shravage, B., Simin, R., Baehrecke, E.H., and Kumar, S. (2012). Relationship between growth arrest and autophagy in midgut programmed cell death in Drosophila. Cell Death Differ *19*, 1299-1307.

Hay, B.A., Wolff, T., and Rubin, G.M. (1994). Expression of baculovirus P35 prevents cell death in *Drosophila*. Development *120*, 2121-2129.

Karres, J.S., Hilgers, V., Carrera, I., Treisman, J., and Cohen, S.M. (2007). The conserved microRNA miR-8 tunes atrophin levels to prevent neurodegeneration in Drosophila. Cell *131*, 136-145.

Li, X., and Carthew, R.W. (2005). A microRNA mediates EGF receptor signaling and promotes photoreceptor differentiation in the Drosophila eye. Cell *123*, 1267-1277.

Li, Y., Wang, F., Lee, J.A., and Gao, F.B. (2006). MicroRNA-9a ensures the precise specification of sensory organ precursors in Drosophila. Genes Dev *20*, 2793-2805.

Sokol, N.S., Xu, P., Jan, Y.N., and Ambros, V. (2008). Drosophila let-7 microRNA is required for remodeling of the neuromusculature during metamorphosis. Genes Dev *22*, 1591-1596.

Teleman, A.A., Maitra, S., and Cohen, S.M. (2006). Drosophila lacking microRNA miR-278 are defective in energy homeostasis. Genes Dev *20*, 417-422.

Usui-Aoki, K., Matsumoto, K., Koganezawa, M., Kohatsu, S., Isono, K., Matsubayashi, H., Yamamoto, M.T., Ueda, R., Takahashi, K., Saigo, K., *et al.* (2005). Targeted expression of Ip3 sponge and Ip3 dsRNA impaires sugar taste sensation in Drosophila. J Neurogenet *19*, 123-141.

Xu, P., Vernooy, S.Y., Guo, M., and Hay, B.A. (2003). The *Drosophila* microRNA mir-14 suppresses cell death and is required for normal fat metabolism. Curr Biol *13*, 790-795.